Structure and Photoluminescence of Nano-ZnO Films Grown on a Si (100) Substrate by Oxygen- and Argon-Plasma-Assisted Thermal Evaporation of Metallic Zn

2005 Chinese Phys. Lett. 22 998

(http://iopscience.iop.org/0256-307X/22/4/061)

Structure and Photoluminescence of Nano-ZnO Films Grown on a Si (100) Substrate by Oxygen- and Argon-Plasma-Assisted Thermal Evaporation of Metallic Zn *

LU Li-Xia(路丽霞)[1,2], TANG Qin-Xin(汤庆鑫)[1], SHAO Chang-Lu(邵长路)[1], LIU Yi-Chun(刘益春)[1,3**]

[1] *Center for Advanced Optoelectronic Functional Material Research, Northeast Normal University, Changchun 130024*

[2] *School of Science, Hebei University of Technology, Tianjin 300130*

[3] *Key Laboratory of Excited State Processes, Changchun Institute of Optics, Fine Mechanics & Physics, Chinese Academy of Sciences, Changchun 130021*

(Received 7 December 2004)

Nano-ZnO thin films were prepared by oxygen- and argon-plasma-assisted thermal evaporation of metallic Zn at low temperature, followed by low-temperature annealing at 300° C to 500° C in oxygen ambient. X-ray diffraction patterns indicate that the nano-ZnO films have a polycrystalline hexagonal wurtzite structure. Raman scattering spectra demonstrate the existence of interface layers between Zn and ZnO. Upon annealing at 400° C for 1 h, the interface mode disappears, and photoluminescence spectra show a very strong ultraviolet emission peak around 381 nm. The temperature-dependent PL spectra indicate that the UV band is due to free-exciton emission.

PACS: 81. 15. Jj, 81. 40. Ef, 81. 07. Bc, 78. 55. Et, 78. 66. Hf

Nano-semiconductor materials are promising candidates for future electronic and photonic devices. In nano-semiconductor materials, carriers are confined in a locational space and concentrated within determined levels, enhancing exciton oscillator strength and light-emission efficiency. ZnO, possessing a wide direct band gap of 3.3 eV at room temperature with a large exciton binding energy of 60 meV, has attracted considerable attention to the applications of ultraviolet light-emitting devices.[1−3] Furthermore, ZnO is one of the "hardest" materials in the II-VI compound family.[4] As a result, ZnO devices do not suffer from dislocation degradation during operation. Many techniques, such as sputtering,[5] reactive thermal evaporation,[6] spray pyrolysis,[7] pulsed laser deposition,[8] metal organic chemical vapour deposition (MOCVD)[9] and molecular beam epitaxy (MBE),[4] have been used to prepare nano-ZnO films. However, low-temperature preparation of stoichiometric nano-ZnO films using these methods is difficult without plasma-assisted techniques. This is because the large binding energy of an oxygen molecule (5.16 eV) and the lower surface mobility of radical cause many oxygen vacancies and voids in films.

In this Letter, we present a simple and economical method to obtain nano-ZnO films by oxygen- and argon-plasma-assisted thermal evaporation of metallic Zn onto a Si substrate at 250°C, followed by thermal annealing from 300°C to 500°C for 1 h in oxygen ambient. The structural and luminescent properties of the samples were studied by employing x-ray diffraction (XRD), Raman scattering and photoluminescence (PL) spectra. A very strong ultraviolet peak near 381 nm and relatively weak emission near 510 nm were observed at room temperature.

The nano-ZnO films used were grown on a Si (100) substrate by plasma-assisted thermal evaporation of metallic Zn. High-purity metallic Zn (99.999%) and a fine-polished Si (100) wafer chemically treated by an RCA process[10] were used as the evaporation source and the substrate, respectively. A turbomolecular pump evacuated the chamber to a base pressure of 3.0×10^{-4} Pa. The substrate temperature was kept at 250°C. Before evaporation, argon plasma generated in the Kaufman ion source was used to etch the Si substrate for 10 min to clean the surface. In this experiment, the energies of all plasmas used were 100 eV and the voltage of the accelerator was 100 V. During the evaporating of Zn, oxygen and argon plasmas were introduced into the reactor chamber. The chamber pressure was held at 2.0×10^{-2} Pa. The growth of the film took 30 min. Subsequently, the sample was cut into four parts. Three parts were respectively annealed in a thermal tube furnace in an oxygen ambient at 300, 400 and 500°C for 1 h. After thermal oxidation, the samples were removed from the furnace and allowed to cool naturally in air. The thickness of the unannealed sample and the samples annealed at 300, 400 and 500°C were measured to be approximately 840 nm, 750 nm, 700 nm and 480 nm by an automatic ellipsometer, respectively. To characterize the structural properties of nano-ZnO films, XRD spectra were measured using a rotating-anode x-ray diffractometer with Cu K_{α_1} radiation of 1.54 Å (D/Max-rA Rigoku).

* Supported by the Hundred Talents Programme of the Chinese Academy of Sciences, the National Natural Science Foundation of China under Grant Nos 60376009 and 60278031, and the Cultivation Fund of the Key Scientific and Technical Innovation Project, Ministry of Education of China (No 704017).

** To whom correspondence should be addressed. Email: ycliu@nenu.edu.cn

Raman scattering measurements were conducted using a J-Y UV-lamb microlaser Raman spectrometer with the 488.0 nm line of an Ar^+ laser as excitation light. To study the UV-band luminescence properties, photoluminescence (PL) spectra were obtained with a He–Cd laser at wavelength 325 nm.

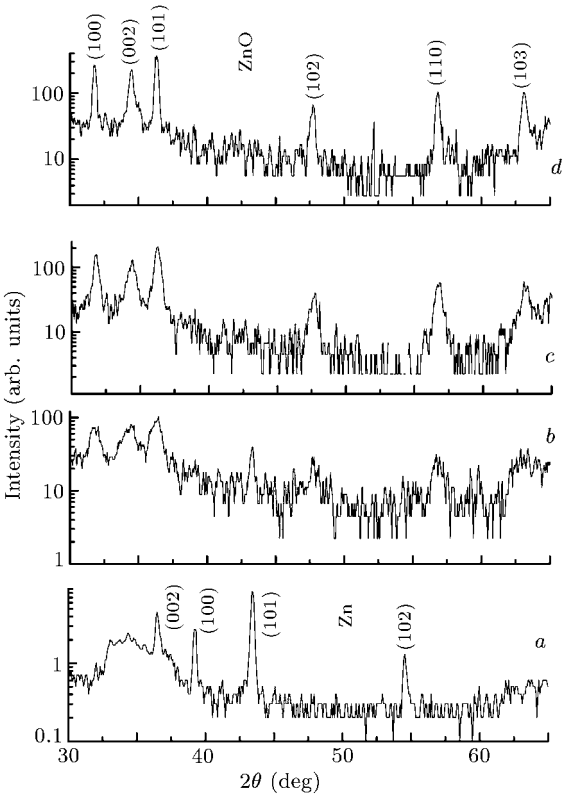

Fig. 1. X-ray diffraction patterns of the ZnO nano-grains grown on Si (100) substrates (a) and the samples annealed at (b) 300, (c) 400, and (d) 500°C.

Figure 1 shows $\theta - 2\theta$ XRD patterns of all the samples, where spectrum a corresponds to the as-grown sample a, and spectra b, c, and d correspond to the samples b, c, and d annealed at 300, 400 and 500°C, respectively. Characteristic Zn peaks are observed in spectrum a at 36.44, 39.20, 43.42 and 54.54°. A broad peak at 31°–38° overlapped by the (100) peak at 31.78°, (002) peak at 34.44° and (101) peak at 36.33° of ZnO with a polycrystalline hexagonal wurtzite structure is observed, which means that a part of Zn transforms to ZnO during annealing. Spectra $b-d$ show that as annealing temperature increases, the Zn peak intensities decrease significantly, while ZnO peak intensities increase and the peaks become sharper due to the increase of ZnO grain sizes. For the sample annealed at 400°C for 1 h, Zn peaks become weaker and weaker, indicating that Zn is mostly transformed to ZnO. The mean ZnO grain size d can be calculated by the Scherrer formula:[11]

$$d = 0.9\lambda/(B\cos\theta), \tag{1}$$

where λ is the x-ray wavelength, B is the full width at half-maximum (FWHM) in radians, and θ is the diffraction angle. For sample a, the mean grain size of Zn is about 3.6 nm. When the samples undergo a thermal annealing process, the mean grain sizes are about 10.8, 15.9 and 19.0 nm for the samples b, c, and d, respectively. The sizes of nano-ZnO grains increase with the increasing annealing temperature, as is expected.

Figure 2 shows the Raman scattering spectra of all the samples. The 438 cm^{-1} and 581 cm^{-1} are attributed to the transverse optical (TO) mode and the longitudinal optical (LO) mode of bulk ZnO,[12] respectively. In curve a of Fig. 2, a new broad band centered at about 530 cm^{-1} between the TO and the LO modes, i.e. interface mode (E_s), is observed, which is from the interface of Zn particles coated with ZnO nano-grains.[13] With the increase of the annealing temperature, the E_s shifts to low wave number with the decrease of the intensity, while the LO mode shifts to high wave number with the increase of the intensity. The frequency of the interface phonon can be calculated by[13]

$$(l+1)[\varepsilon_m - \varepsilon(\omega)]a^{2l+1} - [\varepsilon(\omega) + \varepsilon_m(l+1)]b^{2l+1} = 0, \tag{2}$$

$$\varepsilon(\omega) = \varepsilon_\infty \frac{\omega^2 - \omega_{LO}^2}{\omega^2 - \omega_{TO}^2}, \tag{3}$$

where ε_m is the dielectric constant of the confining medium, ε_∞ is the dielectric constant at high frequency, ω_{LO} and ω_{TO} are the LO and TO frequencies, respectively; a is the radius of Zn sphere, b is the outer radius that is the sum of the Zn sphere radius and the ZnO sphere radius. In our experiment, the Raman spectra were carried out in air, so $\varepsilon_m = 1$. Hence, $\varepsilon_\infty = 3.7$, $\omega_{TO} = 438\ cm^{-1}$ and $\omega_{LO} = 581\ cm^{-1}$. Combining Eqs. (2) and (3), we can obtain the relationship between E_S frequencies and a/b. In terms of theoretical analysis, the E_S frequencies decrease with the increase of the ZnO coating layer thickness, which agrees well with our experimental results. With the increasing annealing temperature, Zn grains transform into ZnO nano-grains, which results in the increasing thickness of the ZnO coating layer, the decreasing radius of Zn sphere and the decreasing interface area between Zn grains and the ZnO coating layer. Thus, the intensity of ZnO modes increases and that of the E_S mode decreases. When the film is annealed at 400°C for 1 h, Zn grains mostly transform to ZnO. The interface mode disappears, only TO and LO modes are observed. This result is quite consistent with the result of XRD. The wave number of the LO mode depends strongly on the diameter d of the ZnO nano-grains. The relationship can be described by[14]

$$d = 2\pi\sqrt{\frac{B}{\Delta\omega}}\text{Å}, \tag{4}$$

where B is a constant and $\Delta\omega$ is the difference between the typical Raman frequency of ZnO ($583\,\mathrm{cm}^{-1}$)[12] and the experimental measurement. The particle diameters obtained by XRD as a function of the inverse $\Delta\omega$ are depicted in Fig. 3. The solid line is the theoretical fit of Eq. (4) to the experimental data. It appears that the diameters given by Eq. (4) are in agreement with those obtained by XRD.

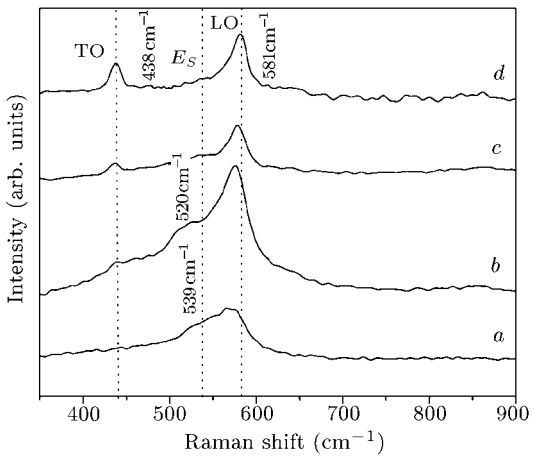

Fig. 2. Raman scattering spectra of (a) as-grown ZnO nano-grains and the samples annealed at different temperatures (b) 300, (c) 400, and (d) 500°C, measured at room temperature with 4880 Å excitation.

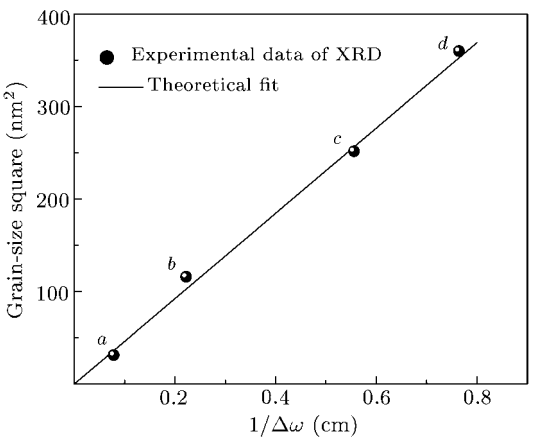

Fig. 3. Particle diameter obtained by XRD as a function of the inverse of $\Delta\omega$. The solid line is the theoretical fit to the experimental data by the equation $d = 2\pi\sqrt{\dfrac{B}{\Delta\omega}}$.

Figure 4 shows the room-temperature PL spectra of all the nano-ZnO thin films. A strong UV emission at about 381 nm and a very weak deep-level emission at about 510 nm are observed. The PL peak at UV band shifts to low energy side when the film is annealed at 300°C. However, when the annealing temperature is higher than 300°C (samples c and d), the peak hardly moves. According to quantum-confinement theory, the energy band gap of a semiconductor will decrease with the increasing crystal size. When the grain size is larger than 8 nm, the quantum-confinement effect turns weak.[15] Therefore, the peak hardly moves when the annealing temperature is higher than 300°C. The visible emissions are composed of two parts, i.e. the green band and the yellow band. It is generally accepted that the green band is associated with oxygen vacancies and interstitial Zn ions[16] and the yellow band is attributed to oxygen interstitial in ZnO lattices.[17] When the sample is annealed at 500°C, the intensity of the visible emissions increases greatly, especially of the green band. It is deduced that more oxygen vacancies and interstitial Zn ions are introduced into the films. A method to evaluate the concentration of structural defects in ZnO is used to compare the PL intensity ratio of the UV near-edge emission to the deep-level emission. The reported PL spectra of ZnO polycrystalline thin films have shown the deep-level emission much stronger than the UV emission, resulting in a relative PL intensity ratio of near zero at room temperature.[4] In our results, the ratio of the UV band to visible emission is 9.6, 10.4, and 3.93 for samples b, c, and d, respectively. When the film is annealed at 400°C for 1 h, the ratio is the maximum, indicating that the film annealed at 400°C has the best crystal quality, due to the fact that this temperature is below the melting point of zinc (419°C). Zinc stays in a solid state and can be oxidized at relative equilibrium conditions.[18] When the temperature reaches to 500°C, which is higher than its melting point, oxidation is carried out at an unstable liquid state. More defects will be introduced into the films, especially oxygen vacancies and interstitial Zn ions. As a result, the weak UV PL emission and intense deep-level emission are observed, as shown in Fig. 4.

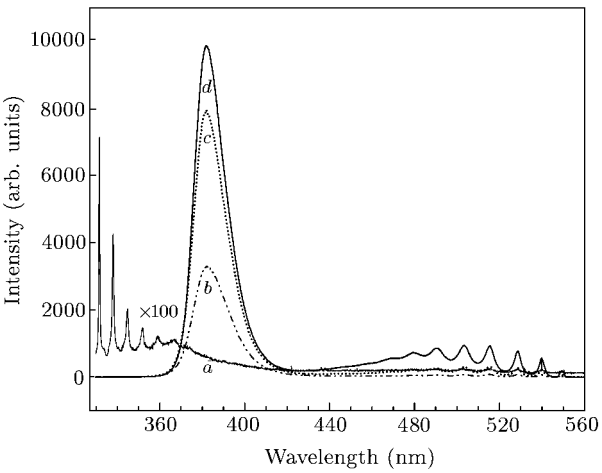

Fig. 4. Luminescence spectra of (a) as-grown ZnO nano-grains and the samples annealed at 300° (b), 400° (c), 500°C (d), measured at room temperature with 3250 Å excitation.

Figure 5 shows the temperature-dependent PL spectra of sample b in the range from 83 K to 300 K.

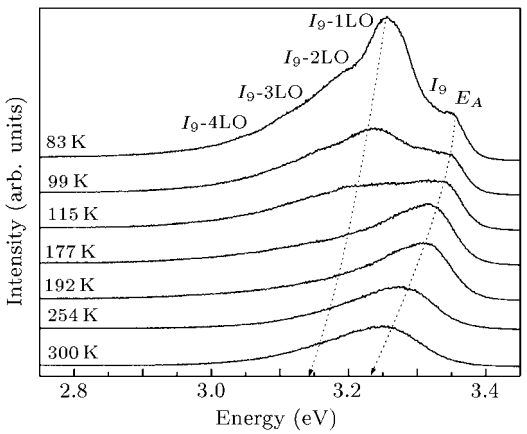

Fig. 5. The dependence of PL spectra of sample b at different temperatures.

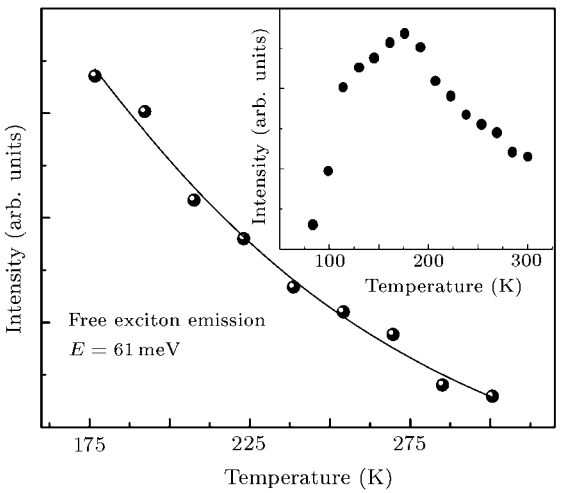

Fig. 6. The PL integrated intensities of peak E_A as a function of measurement temperatures ranging from 177 K to 300 K. The squares represent the experimental data simulated by the theoretical formula $I(T) = I_0/[1 + A\exp(-\Delta E/k_B T)]$. The inset shows the PL integrated intensities of peak E_A as a function of temperatures ranging from 83 K to 300 K.

The peak at 3.35 eV (E_A) can be attributed to free exciton (FE) emission, which will be confirmed by the temperature dependent PL spectra. The peak at 3.33 eV (I_9) is from the neutral accepter bound exciton (BE) emission. Hence, the binding energy of excitons bound to neutral acceptors is estimated to be 20 meV, which agrees well with the reported value.[19] The peaks at 3.26, 3.19, 3.11, and 3.04 eV are from the multiple phonon replica of BE, here the phonon energy is about 60 meV. The dependence of the integrated PL intensity of the FE is illustrated in Fig. 6. With the increasing temperature from 83 K to 177 K, the PL intensity of the FE increases because the bound excitons are thermally ionized to free excitons. When the temperature is higher, the PL is quenched due to the thermal ionization of exciton and thermally activated nonradiative recombination mechanisms, as shown in the inset of Fig. 6. The temperature dependence of the PL intensity can be expressed by[20]

$$I(T) = I_0/[1 + A\exp(-\Delta E/k_B T)], \qquad (5)$$

where ΔE is the activation energy of the thermal quenching process, k_B is the Boltzmann constant, I_0 is the emission intensity at 0 K, T is the thermodynamic temperature, and A is a constant. The solid line in Fig. 6 is the theoretical fit to the experimental data, here $\Delta E = 61$ meV. This value is consistent with the exciton binding energy of 60 meV in bulk ZnO crystals,[3] which indicates that E_A is from free exciton emission.

In summary, we have investigated the structural and photoluminescence properties of ZnO thin films prepared by plasma-assisted thermal evaporation of metallic Zn, using XRD, Raman scattering spectra and PL spectra. The calculations of the size of ZnO grains is obtained by using XRD and Raman spectra, which indicates the existence of nano-ZnO grains. The interface mode is correlated with the annealing temperature. A strong UV emission peak at 381 nm is observed, while the deep-level emission band is barely observed at room temperature. The UV band emission is assigned to excitons. At low growing temperature of 250°C and low annealing temperature of 400°C, a fine nano-ZnO thin film is obtained by plasma-assisted thermal evaporation of metallic Zn.

References

[1] Jing L Q and Xu Z L 2002 *Mater. Sci. Engin.* A **332** 356
[2] Service R F 1997 *Science* **276** 895
[3] Hummer K 1973 *Phys. Status Solidi* **56** 279
[4] Chen Y, Bagnall D M, Koh H J, Park K T, Hiraga K and Zhu Z 1998 *Appl. Phys. Lett.* **84** 3912
[5] Nanto H, Mianmi T and Takata S 1981 *Phys. Status Solidi* A **65** K131
[6] Mprgan H and Brodie D E 1982 *Can. J. Phys.* **60** 1387
[7] Aronovich J, Ortiz A and Bube R H 1979 *J. Vac. Sci. Technol.* **16** 348
[8] Vispute R D, Talyansky V, Choopun S, Sharma R P, Venkatesan T, He M, Tang X, Halpern J B, Spencer M G, Li Y X, Salamanca-Riba L G, Iiiados A A and Jones K A 1998 *Appl. Phys. Lett.* **73** 348
[9] Zhao G L, Lin B X, Hong L, Meng X D and Fu Z X 2004 *Chin. Phys. Lett.* **21** 1381
[10] Kern W and Pwotinen D A 1970 *RCA Rev.* **31** 187
[11] Cullity B D 1978 *Elements of X-ray Diffractions* (Reading, MA: Addison-Wesley) p 102
[12] Damen T C, Porto S P S and Tell B 1966 *Phys. Rev.* **142** 570
[13] Xu J F and Du Y W 1996 *Phys. Lett.* A **215** 215
[14] He Y L, Liu X N and Wang Z C 1992 *Chin. Sci.* A **9** 995
[15] Wu H Z , Qiu D J , Cai Y J, Xu X L and Chen N B 2002 *J. Crys. Growth* **245** 50
[16] Vanheusden K 1996 *J. Appl. Phys.* **79** 7983
[17] Studenikin S A, Golego N and Cocivera M 1998 *J. Appl. Phys.* **84** 2287
[18] Wang Y G, Lau S P, Lee H W, Yu S F, Tay B K, Zhang X H and Hng H H 2003 *J. Appl. Lett.* **94** 354
[19] Presser G J N and Broser I 1998 *Phys. Rev.* B **38** 9746
[20] Jiang D S, Jung H and Ploog K 1988 *J. Appl. Phys.* **64** 1371